Data-Light Oscillation Mode Identification for Fast Stability Assessment of Grid-Tied Converters

Kong, Rui; Sahoo, Subham; Ou, Shuyu; Meng, Xiangyu; Gao, Guoqing; Blaabjerg, Frede

Published in:
I E E E Transactions on Power Electronics

DOI (link to publication from Publisher):
10.1109/TPEL.2025.3556387

Publication date:
2025

Document Version
Accepted author manuscript, peer reviewed version

Data-Light Oscillation Mode Identification for Fast Stability Assessment of Grid-Tied Converters

Rui Kong, *Student Member, IEEE*, Subham Sahoo, *Senior Member, IEEE*, Shuyu Ou, *Student Member, IEEE*, Xiangyu Meng, *Student Member, IEEE*, Guoqing Gao, *Student Member, IEEE*, and Frede Blaabjerg, *Fellow, IEEE*

***Abstract*—Dynamic mode decomposition (DMD) is an effective data-driven oscillation mode identification method for instability identification in grid-tied converters. However, time-consuming computation and empirical setting of parameters limit its practical application in rapid stability assessment. This paper introduces data-light dynamic mode decomposition (DL-DMD) by integrating the conventional dynamic mode decomposition (DMD) algorithm with harmonic state space (HSS) theory, which significantly improves computational speed while providing a bandwidth-oriented interpretation for parameter selection in correspondence with the identifiable frequency range of modes. The effectiveness and advantages of the proposed method are verified through offline analysis and online tests based on an experimental platform.**

***Index Terms*—Grid-tied converter, Oscillation mode identification, dynamic mode decomposition, harmonic state space.**

I. Introduction

GRID-tied converters are widely used in modern power systems as interfaces for renewable energy sources, while the interaction between the grid and power converters may cause harmonic instability issues [1], [2]. Some of the reported incidents in wind farms, photovoltaic plants, and HVDC systems [3], [4] show that oscillations might occur in a short period with poor system damping, causing potential disruptions to the power supply. Hence, real-time stability detection is essential for quantifying instability risks and further mitigating impacts by damping control [5], which requires rapid damping assessment capability.

Model-based stability assessment methods of grid-tied converters aim at detailed modeling of dynamic system characteristics [6], e.g. Nyquist stability criterion based on impedance models [7] and eigenvalue analysis with state space models [8], which can be used for mechanism analysis and instability traceability. Compared to the Nyquist criterion, which merely judges whether the system is stable or not, the eigenvalues extracted from the dynamic matrix in the state space model can reflect the oscillation modes of the system to provide oscillation frequency and damping information [4]. However, model-based approaches require fully transparent system structures and controllers, which are unavailable in black-box regimes [9]. As an extension of the impedance method, impedance measurements can assess system stability by measuring frequency response points without internal information of the converters [10], but the frequency-scan process is time-consuming, and additional harmonic source injection is required. Data-driven oscillation detection methods only using sampled signals are more practical in realistic applications, where fast Fourier transform (FFT) is commonly utilized for oscillation component extraction via spectral analysis having superior computational speed [11], but the Fourier spectrum can only provide frequency properties. Similarly, real-time harmonic extraction techniques such as instantaneous reactive power theory (IRPT) are widely used in active power filters (APF) for harmonic detection and control [12]. However, extracting only the harmonic frequencies of the signal does not allow a stability assessment, since the stability depends on the system damping. Fortunately, the dynamic mode decomposition (DMD) algorithm [13], [14] can approximate the dynamic matrix from measured system signal snapshots to identify eigenvalues (modes) involving both frequency and damping information, where the real part of the identified modes can be used to assess the system stability while the imaginary part works for the oscillation frequency calculation. Compared to other mode identification methods such as Prony [15], eigensystem realization algorithm (ERA) [16] and Matrix pencil (MP) algorithm [17], DMD has a higher accuracy [18], which has been used for power system oscillation identification [19], voltage flicker identification [20], and inertia estimation [21]. Moreover, there are well-defined dynamic matrix and state variables in the DMD algorithm, obtaining a discrete form similar to the state space model, as shown in Fig. 1.

As mentioned previously, state space modeling requires a transparent system configuration with full state variables to obtain an accurate solution [6]. In comparison, the DMD method can identify dynamic properties from the available state signals without full state access [22], but the order of the fitted dynamic matrix must be sufficient to ensure that essential oscillation modes can be identified, such that the rows of the input data matrix representing the system states need to be large enough [23], [24]. However, in real-world applications, the limited number of measurable state signals in small-scale grid-tied converter systems results in insufficient rows of data matrices, especially in the black box conditions, where the controller is unknown and only the converter port signals can be measured. Thus, the data stacking technique [25] is usually employed for data augmentation by time-shifting and stacking of measured time-series signals. However, it causes redundant information and large-size input data matrices at the same time, along with a time-consuming computational process.

Rui Kong, Subham Sahoo, Shuyu Ou, Guoqing Gao & Frede Blaabjerg are with the Department of Energy, Aalborg University, 9220 Aalborg East, Denmark (e-mail: {ruko,sssa,so,gga,fbl}@energy.aau.dk). Xiangyu Meng is with the School of Electrical Engineering, Southwest Jiaotong University, Chengdu 610032, China (e-mail: mengxy@my.swjtu.edu.cn).

This work was supported by the European Union's Horizon 2020 research and innovation program under the Marie Skłodowska-Curie under Grant 955614.

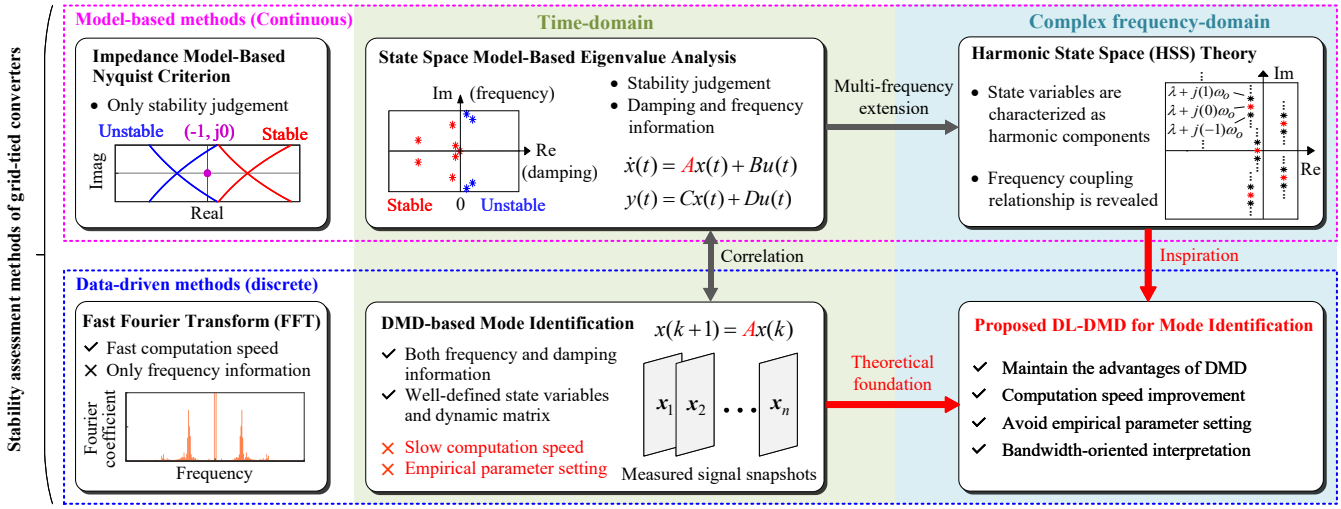

Fig. 1. Comparison of main stability assessment methods for grid-tied converters and the motivation of this paper (DMD: dynamic mode decomposition, DL-DMD: Data-light dynamic mode decomposition.

Moreover, the stacking number has a significant impact on the identification performance, but it is set empirically [18], lacking of physical relevance and theoretical interpretation.

Hence, to address the aforementioned problems and achieve fast oscillation identification for stability assessment of grid-tied converter systems, this paper proposes a novel data-light dynamic mode decomposition (DL-DMD) method inspired by the harmonic state space (HSS) theory. As an analysis framework for linear time-periodic (LTP) systems developed in [26], the HSS theory has been widely used in the stability modeling and analysis of grid-tied power electronic converter systems [27]–[29]. In the HSS theory, time-domain periodic signals are transformed into frequency-domain constants via Fourier decomposition, thereby characterizing state variables as finite harmonic components to reflect the coupling relationship between the frequency components [30]. The multi-frequency state expansion based on Fourier decomposition further complicates the original state space modeling [31], but this process is coincidentally capable of facilitating the achievement of the row expansion of the DMD algorithm while avoiding the data stacking step using empirical parameter setting.

As shown in Fig. 1, in light of the correlation between the DMD algorithm and state space modeling, as well as the fact that HSS is a multi-frequency improved version of the state space method, this paper aims to break through the limitations of the traditional DMD based on time-domain signals, while developing a fast and accurate oscillation mode identification method in the frequency domain by combining HSS theory. To be specific, the sampled signals will be split into multiple groups equally over time. Then, Fourier decomposition is performed in each group to derive Fourier coefficients, which are further used to construct frequency-domain data matrices with a similar mapping relationship to the DMD. In this way, bandwidth-oriented row expansion is provided to specify an identifiable frequency range of modes while computational speed is improved significantly due to the smaller input data size, but without information loss.

The rest of this paper is organized as follows. Section II introduces the basic concepts of the traditional DMD method and its drawbacks. Section III proposes the data-light method with a detailed derivation process and discusses its advantages. In Section III, the proposed mode identification method is assessed and compared with the conventional DMD. In Section IV, an online test is performed for further verification and Section V concludes this paper.

II. DMD for Oscillation Mode Identification

Data-driven oscillation mode identification methods are practical for oscillation detection and stability assessment, where DMD stands out with clearly defined state variables and system dynamic matrix [18], [19]. As shown in Fig. 2(a), a grid-tied three-phase inverter with a virtual synchronous generator(VSG)-based grid forming (GFM) controller is used as the objective system for method verification, where the detailed control diagram and control parameters can be found in [8]. Note that DMD, as a data-driven oscillation mode identification method, can be performed using only sampled signals, thus it is also available in converter systems with other control strategies or even in black-box scenarios with unknown controllers. As shown in Fig. 2(b), based on discrete signal measurements, $x_{a,b}$ $(a = 1, 2, \ldots, m;\ b = 1, 2, \ldots, n)$ is defined as a data element, where m is the number of system states and n represent sampled points with fixed interval Δt, so the sampling frequency $f_s = 1/\Delta t$. Note that the choice of m and n depends on the number of available state signals and the frequency range of interest, respectively. The data snapshot at the b^{th} sampled point is defined as $\mathbf{x}_b = (x_{1,b}, x_{2,b}, ..., x_{m,b})^{\mathsf{T}}$. By gathering the snapshots, a pair of data matrices with a time shift are generated as $\mathbf{X}_1^{n-1} \in \mathbb{R}^{m\times(n-1)} = [\mathbf{x}_1, \mathbf{x}_2, ..., \mathbf{x}_{n-1}]$ and $\mathbf{X}_2^{n} \in \mathbb{R}^{m\times(n-1)} = [\mathbf{x}_2, \mathbf{x}_3, ..., \mathbf{x}_{n}]$, while their mapping matrix (also named as dynamic matrix $\mathbf{A} \in \mathbb{R}^{m\times m}$) governs the inherent dynamic evolution of a discrete linear system:

$$\mathbf{X}_2^n = \mathbf{A}\mathbf{X}_1^{n-1}, \mathbf{A} = \mathbf{X}_2^n(\mathbf{X}_1^{n-1})^{\dagger} \tag{1}$$

To calculate pseudo-inverse matrix $(\mathbf{X}_1^{n-1})^{\dagger}$, singular value decomposition (SVD) with the reduction rank r (determined by the number of effective singular values) is implemented as:

$$\mathbf{X}_1^{n-1} = \mathbf{U}\mathbf{\Sigma}\mathbf{V}^{\mathsf{T}} \tag{2}$$

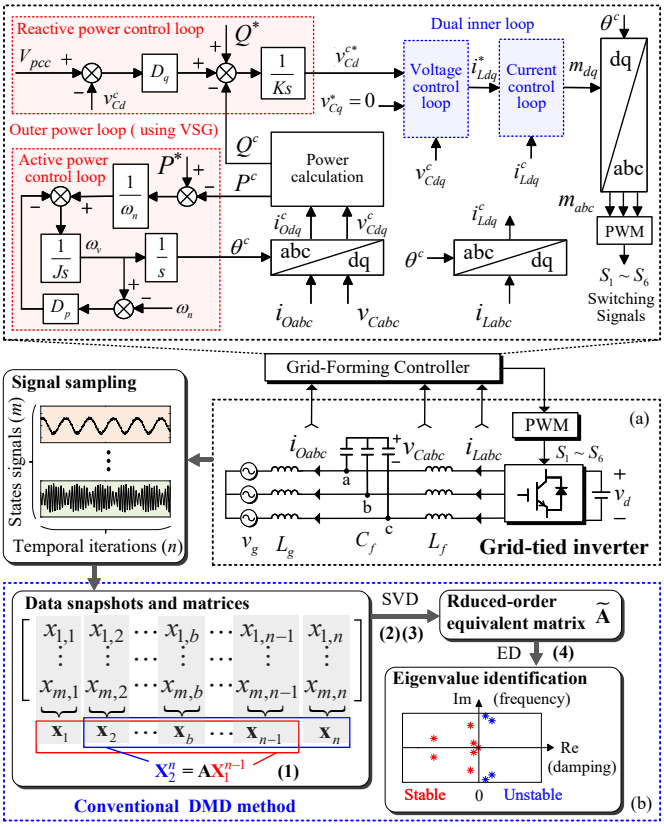

Fig. 2. Schematic of (a) stand-alone grid-tied inverter system with a virtual synchronous generator(VSG)-based grid forming (GFM) controller and (b) conventional dynamic mode decomposition (DMD) method for oscillation mode identification (m: number of measured state signals, n: number of total sampled points, $x_{a,b}$: data value of the a^{th} state signal at the b^{th} sampling point, $(a = 1, 2, \ldots, m;\ b = 1, 2, \ldots, n)$, $\mathbf{x}_b$: data snapshot at the b^{th} sampled point, SVD: singular value decomposition, ED: eigen-decomposition).

where, the obtained singular vectors $\mathbf{U} \in \mathbb{R}^{m\times r}$ and $\mathbf{V} \in \mathbb{R}^{(n-1)\times r}$ are unitary matrices, $\mathbf{\Sigma} \in \mathbb{R}^{r\times r}$ is the diagonal matrix of singular values, and the superscript 'T' represents the matrix transpose. Then, a reduced-order equivalent matrix $\tilde{\mathbf{A}}$ of initial full dynamic matrix $\mathbf{A}$ can be derived by projecting $\mathbf{A}$ onto an $\mathbf{U}$ basis subspace of dimension r as:

$$\tilde{\mathbf{A}} = \mathbf{U}^{\mathsf{T}}\mathbf{A}\mathbf{U} = \mathbf{U}^{\mathsf{T}}\mathbf{X}_2^n\mathbf{V}\mathbf{\Sigma}^{-1} \tag{3}$$

Next, the eigen-decomposition (ED) of $\tilde{\mathbf{A}}$ is performed as:

$$\tilde{\mathbf{A}} = \mathbf{W}\mathbf{\Lambda}\mathbf{W}^{-1} \tag{4}$$

where, $\mathbf{W}$ is the eigenvectors, and $\mathbf{\Lambda}$ is the diagonal matrix consisting of eigenvalues $(\lambda_1, \lambda_2, \cdots, \lambda_r)$, also denoted as identified oscillation modes. The presence of negative damping modes (with a positive real part larger than 0, i.e., in the right-half complex plane) will lead to divergent oscillations, but the system will be stable if all modes are in the left-half complex plane with negative real parts.

For large-scale networks with a large number of inverters, there is a sufficient number of measurable signals m, and DMD can be employed for accurate oscillation mode identification. However, for small-scale grid-tied converter systems such as the stand-alone inverter as shown in Fig. 2(a), the measurable signals are limited, especially in black box scenarios where the controller is unknown, causing the unavailability of the DMD algorithm. For example, if there is only one sampled state signal (m = 1), each data snapshot will have one element according to Fig. 2(b), and the row number of the dynamic matrix $\mathbf{A}$ is 1. As a result, the maximum number of identifiable eigenvalues will be 1, which is insufficient to reflect system dynamics. To ensure accurate results containing all critical modes, the data-stacking technique is commonly employed as data pre-processing for DMD [18], [20], [23]–[25]. As shown in Fig. 3, after determining the stacking number h, the 1st to $(n-h+1)^{\text{th}}$ data snapshots are set to the first row, the 2nd to $(n-h+2)^{\text{th}}$ data snapshots are set to the second row, and so on until the number of rows in the stack reaches h. As a result, augmented data matrices $\mathbf{X}_{aug,1}, \mathbf{X}_{aug,2} \in \mathbb{R}^{mh\times(n-h)}$ are obtained with more rows, while the dynamic mapping remains unchanged as:

$$\mathbf{X}_{aug,2} = \text{diag}\begin{bmatrix}\mathbf{A} & \cdots & \mathbf{A}\end{bmatrix}\mathbf{X}_{aug,1} \tag{5}$$

Thus, by replacing the original input data matrices $\mathbf{X}_1^{n-1}$, $\mathbf{X}_2^n$ in Fig. 2(b) with augmented data matrices $\mathbf{X}_{aug,1}, \mathbf{X}_{aug,2}$, the row number of the fitted dynamic matrix can be increased for extracting sufficient modes, while the dynamic mapping relationship with valid information of the original data is unchanged. However, stacking number h, as a key parameter, needs to be set manually based on experience, where a small h leads to poor accuracy, while a larger h brings the augmented data matrices with large sizes and much information redundancy, resulting in low computational speed. Hence, stacking number h is usually determined based on the original data sizes, considering the reconciliation of the contradiction between accuracy and efficiency, but itself lacks a clear physical significance. Furthermore, the computational burden of the conventional DMD with data stacking increases rapidly with the size of the original data, for instance, when a long sampling window and a high sampling frequency are adopted for identifying wide-band oscillations.

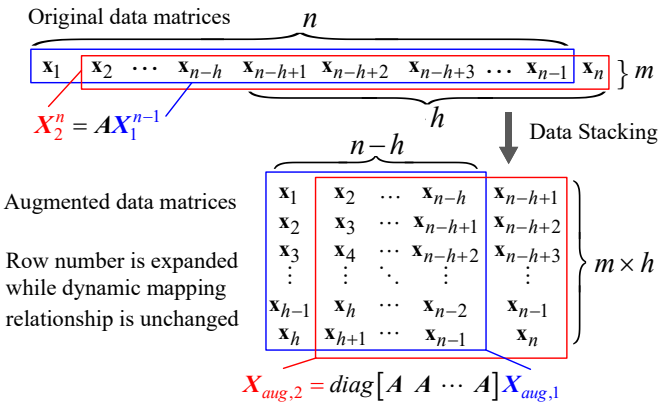

Fig. 3. Diagram of data-stacking technique — data matrices are augmented with higher row numbers to ensure that all critical modes can be identified, but leading to the large size of input data matrices (m: number of measured state signals, n: number of total sampled points, h: stacking number, $\mathbf{x}_b$: data snapshot at the b^{th} sampled point, $b = 1, 2, \ldots, n$).

III. Proposed Method

A. Data-Light Mode Identification

Inspired by the harmonic state space (HSS) theory [26], the data-light mode identification method proposed in this paper aims to reduce the input data size without information loss, and provide a Fourier decomposition-based system state expansion with bandwidth-oriented interpretation in the DMD algorithm, avoiding the data stacking step.

The HSS theory has been applied in the grid-tied converter modeling [27]–[29], where the time-domain states and dynamic matrix are expanded into complex Fourier series with the exponentially modulated periodical signal shown as:

$$\mathbf{x}(t) = e^{st}\sum_{k\in Z}\mathbf{X}_k e^{jk\omega_0 t}, \mathbf{A}\,(t) = \sum_{k\in Z}\mathbf{A}_k e^{jk\omega_0 t} \tag{6}$$

where, s is the Laplace operator, j is the imaginary unit, ω_0 is the fundamental angular frequency, $\mathbf{X}_k \in \mathbb{R}^{m\times 1}$ and $\mathbf{A}_k \in \mathbb{R}^{m\times m}$ are the k^{th} Fourier coefficients. ($\mathbf{X}_k$ is different from the snapshot $\mathbf{x}_b$ defined in Section II-A). The relationship representation between the Fourier coefficients of the system states in a compact matrix form can be obtained in the s-domain, as:

$$s\mathcal{X} = (\mathcal{A} - \mathcal{N})\,\mathcal{X} \tag{7}$$

where, $\mathcal{A}$, $\mathcal{N}$, and $\mathcal{X}$ are infinite, and $\mathcal{A}$ is a Toplitz matrix, which can be denoted as:

$$\mathcal{X} = \begin{bmatrix} \vdots \\ \mathbf{X}_{-1} \\ \mathbf{X}_0 \\ \mathbf{X}_1 \\ \vdots \end{bmatrix}, \mathcal{A} = \begin{bmatrix} \ddots & \vdots & \vdots & \vdots & \iddots \\ \cdots & \mathbf{A}_0 & \mathbf{A}_{-1} & \mathbf{A}_{-2} & \cdots \\ \cdots & \mathbf{A}_1 & \mathbf{A}_0 & \mathbf{A}_{-1} & \cdots \\ \cdots & \mathbf{A}_2 & \mathbf{A}_1 & \mathbf{A}_0 & \cdots \\ \iddots & \vdots & \vdots & \vdots & \ddots \end{bmatrix},$$

$\mathcal{N} = diag\left[\cdots\ -j2\omega_0\mathbf{I}\ \ -j\omega_0\mathbf{I}\ \ 0\ \ j\omega_0\mathbf{I}\ \ j2\omega_0\mathbf{I}\ \cdots\right]$, and $\mathbf{I} \in \mathbb{R}^{m\times m}$ is the unit matrix. Then, the system stability can be assessed with the eigenvalues of matrix $\mathcal{A} - \mathcal{N}$.

The principle of DMD is clear in the time domain, while the HSS theory is developed in the s-domain. Thus, the key step of the proposed data-light method lies in constructing a mapping relationship between system states in the form of Fourier coefficients, which is also similar to (1) in the DMD algorithm. As shown in Fig. 4(a), the initial sampling data of the time-domain state signal are equally divided into multiple groups regarding fundamental frequency periods ($T_0 = 0.02$ seconds). Hence, the number of sampled points p in each data group and the total group number q can be calculated as:

$$\begin{cases} p = T_0 f_s \\ q = n/p \end{cases} \tag{8}$$

where, n is the number of total sampled points, f_s is the sampling frequency. Note that the number of sampled signals m is assumed to be 1 for simplifying the expression in Fig. 4(a), but the method works as well with other values of m, which just increases the number of matrix rows.

FFT will be applied in each group to obtain sets of Fourier coefficients ($\mathcal{X}_1$, $\mathcal{X}_2$, $\cdots$, $\mathcal{X}_q$), which are used as each column of the contructed input data matrix. On this basis, discretization of (7) is carried out by transforming it into the z-domain using the Tustin method as:

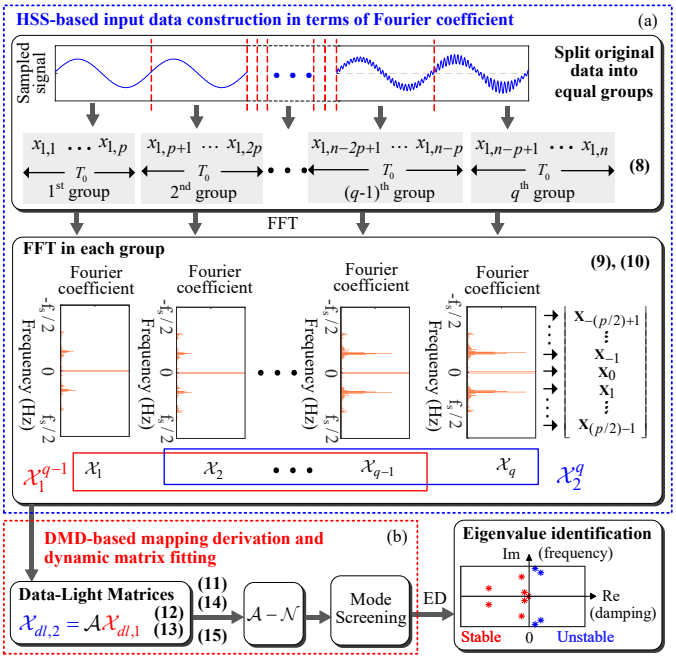

Fig. 4. Schematic of the proposed DL-DMD method for oscillation mode identification (n: number of total sampled points, p: number of sampled points in each data group, q: number of data groups, T_0: fundamental frequency period, $\mathbf{X}_k$: k^{th} Fourier coefficient, $\mathcal{X}_i$: data snapshot in form of Fourier coefficients at i^{th} data group, $\mathcal{X}_{dl,1}$ and $\mathcal{X}_{dl,2}$: derived data-light data matrices fed into DMD, $\mathcal{A} - \mathcal{N}$: final matrix used for extracting eigenvalues, ED: eigen-decomposition).

$$\frac{2(z-1)}{T_0(z+1)}\mathcal{X} = (\mathcal{A} - \mathcal{N})\,\mathcal{X} \tag{9}$$

Then, the inverse z-transform of (9) is performed as:

$$2(\mathcal{X}_{i+1} - \mathcal{X}_i) = (\mathcal{A} - \mathcal{N})\,T_0(\mathcal{X}_{i+1} + \mathcal{X}_i) \tag{10}$$

where, $\mathcal{X}_i$ can be defined as the data snapshot in the form of Fourier coefficients at the i^{th} group ($i = 1, 2, \ldots, q$) with a fixed time interval T_0, and the row number of $\mathcal{X}_i$ is limited due to discrete sampling frequency. Considering the symmetry, there is $\mathcal{X}_i = [\ \mathbf{X}_{-\frac{p}{2}+1}\ \cdots\ \mathbf{X}_{-1}\ \ \mathbf{X}_0\ \ \mathbf{X}_1\ \cdots\ \mathbf{X}_{\frac{p}{2}-1}\ ]^{\mathsf{T}} \in \mathbb{R}^{m(p-1)\times 1}$. Thus, two matrices with a time shift are generated as $\mathcal{X}_1^{q-1} = [\mathcal{X}_1, \mathcal{X}_2, ..., \mathcal{X}_{q-1}]$, $\mathcal{X}_2^{q} = [\mathcal{X}_2, \mathcal{X}_3, ..., \mathcal{X}_q] \in \mathbb{R}^{m(p-1)\times(q-1)}$. Correspondingly, the range of elements in the matrix $\mathcal{N}$ is limited as:

$$\begin{aligned}\mathcal{N} = \text{diag}\big[\ &(-\tfrac{p}{2}+1)j\omega_0\mathbf{I}\ \cdots\ -j\omega_0\mathbf{I}\ \ 0\ \ j\omega_0\mathbf{I} \\ &\cdots\ (\tfrac{p}{2}-1)j\omega_0\mathbf{I}\ \big]\end{aligned} \tag{11}$$

where, $\mathbf{I} \in \mathbb{R}^{m\times m}$ is the unit matrix, and it will be a constant 1 if m = 1.

So far, the HSS-based data construction is finished, which needs further derivation to obtain a mapping relationship similar to the DMD algorithm for dynamic matrix fitting and eigenvalue identification, as shown in Fig. 4(b). Based on the constructed data matrices, (12) can be obtained from (10) as:

$$2(\mathcal{X}_2^q - \mathcal{X}_1^{q-1}) = (\mathcal{A} - \mathcal{N})\,T_0(\mathcal{X}_2^q + \mathcal{X}_1^{q-1}) \tag{12}$$

Furthermore, (12) can be reorganized into a form similar to (1) in the DMD algorithm as:

$$\underbrace{2(\mathcal{X}_2^q - \mathcal{X}_1^{q-1}) + \mathcal{N}T_0(\mathcal{X}_2^q + \mathcal{X}_1^{q-1})}_{\mathcal{X}_{dl,2}} = \mathcal{A}\underbrace{T_0(\mathcal{X}_2^q + \mathcal{X}_1^{q-1})}_{\mathcal{X}_{dl,1}} \tag{13}$$

Therefore, a pair of data matrices, $\mathcal{X}_{dl,1}$ and $\mathcal{X}_{dl,2} \in \mathbb{R}^{m(p-1)\times(q-1)}$, are obtained with the mapping matrix $\mathcal{A}$ to be approximated. The DMD algorithm can be applied similarly to obtain reduced-order matrix $\tilde{\mathcal{A}} \in \mathbb{R}^{r'\times r'}$ as:

$$\tilde{\mathcal{A}} = \mathcal{U}^{\mathsf{T}}\mathcal{X}_{dl,2}\mathcal{V}\mathbf{\Sigma}^{-1} \tag{14}$$

where, $\mathcal{U} \in \mathbb{R}^{m(p-1)\times r'}$ and $\mathcal{V} \in \mathbb{R}^{(q-1)\times r'}$ are the unitary matrices, and $\mathbf{\Sigma} \in \mathbb{R}^{r'\times r'}$ is the diagonal matrix of singular values in the SVD of $\mathcal{X}_{dl,1}$ (i.e., $\mathcal{X}_{dl,1} = \mathcal{U}\mathbf{\Sigma}\mathcal{V}^{\mathsf{T}}$). r' is the number of effective singular values.

However, according to HSS theory, the eigenvalues are extracted from the matrix $\mathcal{A} - \mathcal{N}$, so the derived $\tilde{\mathcal{A}}$ needs to be transformed back to the full matrix $\mathcal{A} \in \mathbb{R}^{m(p-1)\times m(p-1)}$ as:

$$\mathcal{A} = \mathcal{U}\tilde{\mathcal{A}}\mathcal{U}^{\mathsf{T}} \tag{15}$$

Finally, after combining (11) and (15), the system eigenvalues can be identified from the matrix $\mathcal{A} - \mathcal{N}$ by eigendecomposition for stability assessment. It is worth mentioning that, the real-part values of the identified eigenvalues (representing damping) need to be multiplied by 2 for correction, due to the bilateral Fourier coefficients obtained by the FFT. Moreover, $\mathcal{A} - \mathcal{N}$ cannot be directly fitted as a whole from (12), since the matrix $\mathcal{N}$ must satisfy its physical constraint, i.e., $\mathcal{N}$ exists as a diagonal matrix and the diagonal elements are imaginary numbers representing different frequency components. Due to the presence of $\mathcal{N}$, each frequency component in the Fourier spectrum corresponds to an initial eigenvalue on the imaginary axis, which helps to visualize the identifiable frequency range, but makes it difficult to distinguish critical stability modes (in a small neighborhood of the imaginary axis). To address this issue, the elements on the diagonal of the matrix $\mathcal{A} - \mathcal{N}$ can be screened and set to zero if the absolute value of real part is less than a tiny number ϵ such as $1e^{-8}$. Considering the potential spectrum leakage issue of FFT, the obtained data snapshots $\mathcal{X}_i$ need to be filtered by setting the Fourier coefficients smaller than the threshold (e.g., 1) to zero, which can also improve the noise immunity. At the same time, the sparsity of the fitted matrix $\mathcal{A}$ can be facilitated to further accelerate the computational speed.

B. Comparison and Discussion

Using the HSS theory as a foundation, the proposed data-light method features the advantages of DMD and FFT, while the shortcomings of DMD are ingeniously avoided. Comparison between the conventional DMD and the proposed DL-DMD is summarized in Table I.

The proposed method constructs a pair of data matrices, $\mathcal{X}_{dl,1}$ and $\mathcal{X}_{dl,2}$, with smaller sizes due to grouped Fourier transform, improving computational speed but without information loss. Moreover, by comparing Fig. 2(b) and Fig. 4(a), it can be found that the row expansion in the conventional DMD method is achieved by data stacking step with empirically manual setting of parameter h, but for the proposed DL-DMD method, the rows of the constructed data matrix are expanded in the form of Fourier coefficients, so a bandwidth-oriented interpretation of matrix rows is provided according to the Fourier bilateral spectrum that the maximum frequency f_{max} of identifiable modes is determined as:

TABLE I
COMPARISON OF CONVENTIONAL DMD AND PROPOSED DL-DMD METHOD.

Category \ Method	Conventional DMD [13], [14], [18]–[21]	Proposed DL-DMD
Data form	Signal values in the time domain	Laplace coefficients in the frequency domain
Input data matrices	$\mathbf{X}_{aug,1}, \mathbf{X}_{aug,2}$	$\mathcal{X}_{dl,1}, \mathcal{X}_{dl,2}$
Row × column of data matrices	$mh \times (n-h)$	$m(p-1)\times(q-1)$ or $m(2c+1)\times(q-1)$
Sizes of data matrices	Large	Small
Computational speed	Low	High
Identification accuracy	High	High
Tunable parameters	Stacking number h	Truncation number c
Interpretation of row expansion	×	$f_{max} = f_s/2$ or $f_{max} = c/T_0$

m: number of measured state signals, n: number of total sampled points, h: stacking number, p: number of sampled points in each data group, q: number of data groups, c: truncation number, T_0: fundamental frequency period, f_s: sampling frequency, f_{max}: maximum frequency of identifiable modes.

$$f_{\max} = \begin{cases} p/(2T_0) = f_s/2, & \text{without truncation} \\ c/T_0, & \text{with truncation} \end{cases} \tag{16}$$

where, c is defined as the truncation number. When there is no truncation, $c = p/2$ and f_{max} equals the Nyquist frequency $f_s/2$. However, when truncation is performed, there is $\mathcal{X}_i = [\ \mathbf{X}_{-c}\ \cdots\ \mathbf{X}_{-1}\ \ \mathbf{X}_0\ \ \mathbf{X}_1\ \cdots\ \mathbf{X}_c\ ]^{\mathsf{T}}$, with the row number of $\mathcal{X}_i$ being $m(2c+1)$, as shown in Fig. 5. From the derivation of (10) to (15), it can be seen that $\mathcal{A}$ has the same row number as $\mathcal{X}_i$, and after the same truncation of $\mathcal{N}$ as $\mathcal{N} = \text{diag}\left[\ -cj\omega_0\mathbf{I}\ \cdots\ -j\omega_0\mathbf{I}\ \ 0\ \ j\omega_0\mathbf{I}\ \cdots\ cj\omega_0\mathbf{I}\ \right]$, the maximum frequency of eigenvalues identified from $\mathcal{A} - \mathcal{N}$ will be limited to c/T_0. Therefore, setting truncation can further reduce the matrix size to improve computational speed, but also limit f_{max}, resulting in the failure to identify potential oscillations with frequencies higher than c/T_0. However, if the upper limit of the oscillation of interest is known, c can be set accordingly to shorten the computation time for faster stability assessment. In summary, the selection of the tunable parameter c depends on the oscillation frequency range of interest and the requirement of computational speed.

It is worth mentioning that, this paper focuses on the small-scale systems with a limited number m of measurable signals. If m increases to be large (for example, in a large-scale network with a lot of inverters), the aforementioned advantages of the proposed DL-DMD method will be weakened. To be specific, with sufficient m, conventional DMD can be implemented without data stacking, while the row number of data matrices used in DL-DMD will be very large according to Table I, thereby reducing computational speed. However, even in large-scale networks with a lot of inverters, compared to using the conventional DMD method-based mode identification by collecting all measurable signals, if the proposed DL-DMD method can be performed by sampling the grid-connected port voltages or currents of each inverter, it will still have faster computational speed and avoid inter-device communications.

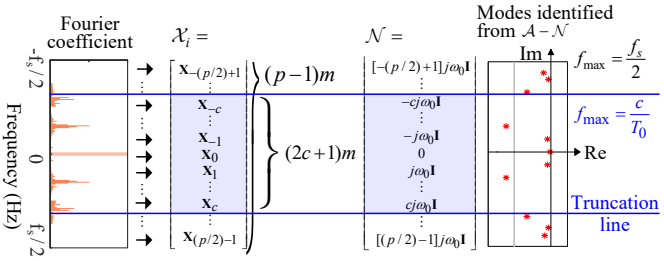

Fig. 5. Fourier decomposition-based row expansion and truncation of the data matrix with bandwidth-oriented interpretation in the proposed DL-DMD method (m: number of measured state signals, p: number of sampled points in each data group, c: truncation number, f_s: sampling frequency, T_0: fundamental frequency period, ω_0: fundamental angular frequency, $\mathbf{X}_k$: k^{th} Fourier coefficient, $\mathcal{X}_i$: data snapshot in the form of Fourier coefficients at i^{th} data group, f_{max}: maximum frequency of identifiable modes, $\mathcal{A}$ - $\mathcal{N}$: final matrix used for extracting eigenvalues).

IV. Offline Verifications

To validate the effectiveness and advantages of the proposed method, offline tests are first performed in this section. After collecting the original data, the proposed DL-DMD method and conventional DMD are tested and compared, where algorithms are performed on a host computer with Intel(R) Core(TM) i5-1135G7 @2.40GHz, 16.0 GB(RAM), and 64-bit operating system.

A. Test Using Composite Signal with Defined Components

A composite signal with well-defined components as shown in (17) is employed for preliminary tests to demonstrate the accuracy of the proposed method in identifying oscillation modes involving frequency and damping information. Assuming that the sampled AC voltage signal $V_s(t)$ contains divergent or decaying oscillation components in addition to the fundamental frequency component, which is shown as:

$$V_s(t) = V_0\cos(\omega_0 t) + V_1 e^{\sigma_1 t}\cos(\omega_1 t) + V_2 e^{\sigma_2 t}\cos(\omega_2 t) \tag{17}$$

where, V_0 is the magnitude of AC voltage with fundamental frequency, V_1 and V_2 are the magnitude of two oscillation components, ω_0 is the fundamental angular frequency, ω_1 and ω_2 are the angular frequency of two oscillation components, σ_1 and σ_2 can reflect the damping of two oscillation components. For the composite signal as shown in (17), the true modes are $(0, \pm j\omega_0)$, $(\sigma_1, \pm j\omega_1)$, and $(\sigma_2, \pm j\omega_2)$.

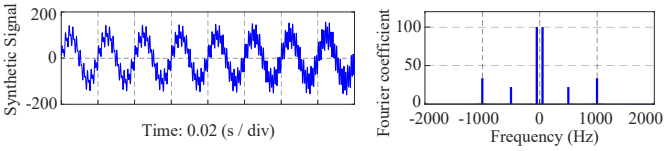

Fig. 6. Composite signal used for preliminary offline test and its bilateral Fourier spectrum, which contains a fundamental frequency component at 50 Hz, a decaying oscillation component at 500 Hz, and a divergent oscillation component at 1000 Hz.

The used composite signal and its corresponding bilateral Fourier spectrum are shown in Fig. 6, where the signal length is 0.16 seconds, and the time step is $5e^{-5}$ seconds, i.e., the sampling frequency is 20 kHz, so the number of measured state signals $m = 1$, and the number of total sampled points $n = 3200$. Further, the total group number q and the number of sampled points p in each data group can be calculated as $q = 8$ and $p = 400$ according to (8). The other signal parameters are set to $V_0 = 100$ (V), $V_1 = 30$ (V), $V_2 = 20$ (V), $\omega_0 = 2\pi \times 50$ (rad/s), $\omega_1 = 2\pi \times 500$ (rad/s), $\omega_2 = 2\pi \times 1000$ (rad/s), $\sigma_1 = -4$, $\sigma_2 = 6$. Admittedly, FFT can extract all frequency information of the composite signal (50 Hz, 500 Hz, and 1000 Hz), but it cannot provide the damping information to reflect the variation trend of each signal component, which plays an important role in stability assessment. Thus, the mode identification methods that can extract both frequency and damping information are more applicable for stability assessment.

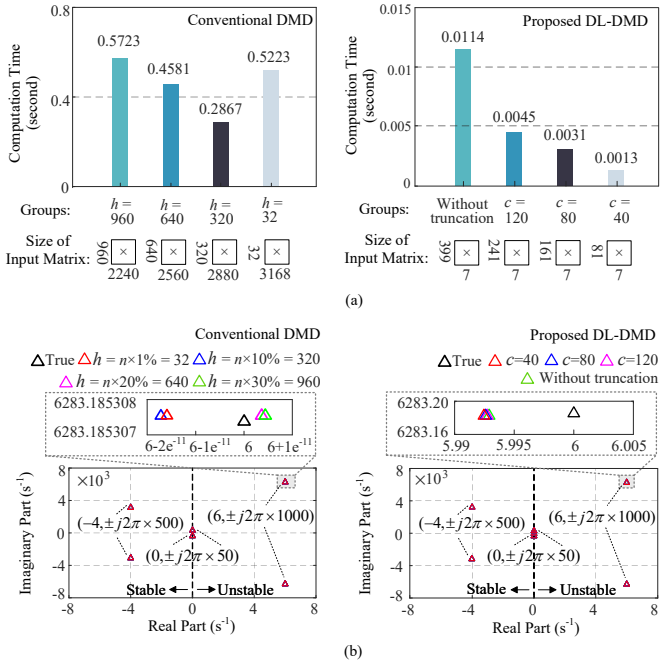

Fig. 7. Performance of the conventional DMD method and the proposed DL-DMD method using a composite signal in terms of (a) computational time and (b) identification accuracy — both DMD and DL-DMD can accurately identify oscillation modes, but the computation speed of DL-DMD is significantly faster than that of DMD (n: number of total sampled points, h: stacking number for DMD, c: truncation number for DL-DMD).

For oscillation mode identification of the composite signal via the conventional DMD with the data-stacking step, after setting stacking number h progressively as 1%, 10%, 20%, and 30% of the number of original sampled points n, i.e., 32, 320, 640, and 960, the data matrix sizes can be derived from Table I, which are given in the left side of Fig. 7(a) with the corresponding computation time (average time of 100 executions). It can be found that the computation time of DMD is in the order of 0.1 seconds. The eigenvalue identification results of DMD as shown in the left side of Fig. 7(b) indicate that the three oscillation modes identified by the DMD are almost the same as the true modes in the composite signal, i.e., fundamental frequency mode at 50 Hz with constant amplitude (real part equals 0), stable oscillation mode at 500 Hz with positive damping (real part equals -4), and unstable oscillation mode at 1000 Hz with negative damping (real part

equals 6). However, the long computation time makes DMD incapable of meeting the demand for rapid identification in real applications.

In comparison, when using the proposed DL-DMD, the computation time (containing the total overhead of FFT and DL-DMD) is significantly shortened to milliseconds due to smaller data matrix sizes as shown in the right side of Fig. 7(a). The mode identification results of DL-DMD are shown in the right side of Fig. 7(b), where three modes of the composite signal can also be identified accurately. Although there is a small error between the identified damping and the true value, it is within acceptable ranges (smaller than 0.01). It is worth mentioning that the modes present on the (0, $j0$) point are brought due to the initial eigenvalue from the matrix $\mathcal{N}$ on the imaginary axis being screened and set to zero. Moreover, identification results without screening of modes on the imaginary axis are shown in Fig. 8 to demonstrate the impact of the truncation number c on the maximum frequency range f_{max} of the identifiable modes. It can be seen that, if no truncation number c is set, the maximum identifiable frequency range f_{max} equals the Nyquist frequency (10 kHz), while the computational time is 11.4 milliseconds according to Fig. 7. Furthermore, if c is set to 120, 80, and 40, f_{max} will be limited to 6, 4, and 2 kHz without loss of identification accuracy, while the computational time is further shortened to 4.5, 3.1, and 1.3 milliseconds. Thus, the results in Fig. 8 verify the bandwidth-oriented interpretation of the only tunable parameter c in the proposed DL-DMD method, which has been presented in Equation (16) and Fig. 5.

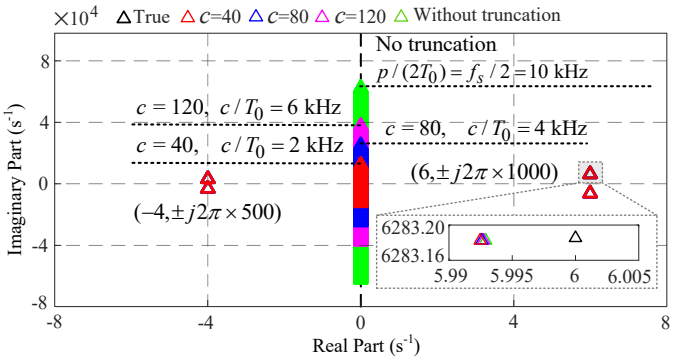

Fig. 8. Maximum frequency range (bandwidth) of identifiable modes can be specified in the proposed DL-DMD method by setting truncation number c (T_0: fundamental frequency period).

To further highlight the advantages of the proposed method in terms of computational speed, the computational times of the conventional DMD and the DL-DMD with different input data sizes (by changing the length of the composite signal) are compared in Fig. 9. It can be seen that, as the data amount progressively increases from 3200 to 12800, the computation time of the DMD almost exponentially increases, but the computational time of DL-DMD increases slightly and linearly. DL-DMD can ensure a fast computational speed even with input data amounts beyond 10000. Therefore, the benefits of DL-DMD are more evident for larger-scale input data in the case of high sampling frequency and long sampling window.

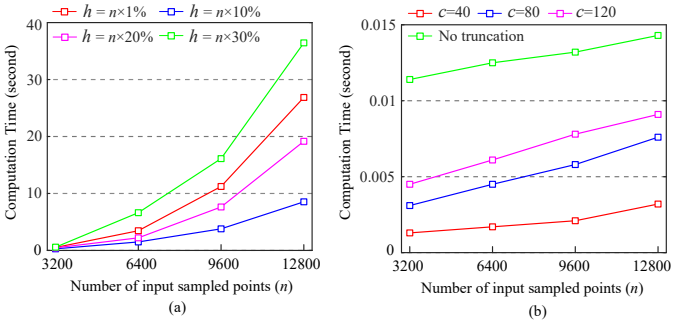

Fig. 9. Computational speed comparison between (a) conventional DMD method and (b) proposed DL-DMD method with different input data sizes — DL-DMD has a fast computational speed even with large input data sizes (h: stacking number, c: truncation number).

B. Test with Experimental Signal

Considering more realistic application scenarios, an experimental signal is sampled from a downscaled experimental platform as shown in Fig. 10(a) and used for further verification. The experimental setup is built based on the system configuration of the grid-tied three-phase inverter as shown in Fig. 2(a), using the VSG-based GFM controller, where irrational control parameters or control delays might lead to high-frequency resonance issues [32], [33]. The phase "a" of AC-side output voltage v_{ca} is used as the measured signal when divergent high-frequency resonance around 1.5 kHz occurs, as shown in Fig. 10(b). The dataset is collected in a window of 0.16 seconds with sampling frequency f_s of 20 kHz (i.e., $m = 1$, $n = 3200$, $p = 400$, $q = 8$).

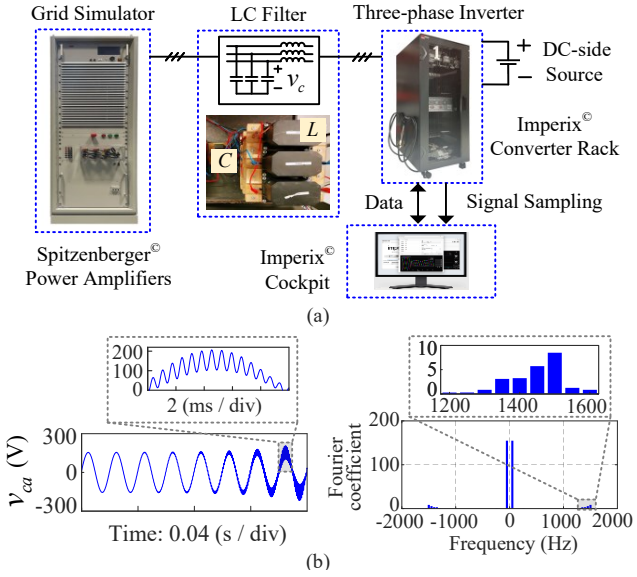

Fig. 10. Experimental setup of (a) downscaled grid-tied three-phase inverter and (b) sampled high-frequency resonance signal for mode identification and its bilateral Fourier spectrum.

The computation time and identified oscillation modes of the measured signal using the conventional DMD and the proposed DL-DMD are shown in Fig. 11(a) and Fig. 11(b) respectively, where the computation time results are similar to that in Fig. 7(a) due to the same size of the original input data ($n = 3200$). It can be found from the left side of Fig. 11(a) that both large and small h (stacking number) will extend the computation time of the conventional DMD

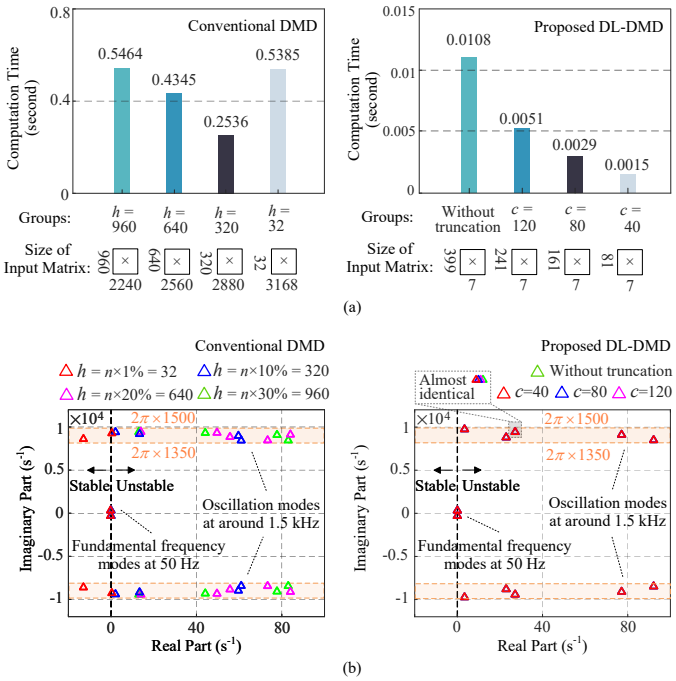

Fig. 11. Performance of the conventional DMD method and the proposed DL-DMD method using a measured signal in terms of (a) computational speed and (b) mode identification — the selection of stacking number h imposes uncertain impacts on the computation speed and mode identification accuracy of DMD, but the impact of truncation number c on algorithm performance of DL-DMD is regular and interpretable.

method. Moreover, the left side of Fig. 11(b) indicates that parameter h affects the mode identification results of the measured real oscillation signal. When h = 960, 640, or 320, the five dominant high-frequency modes at around 1.5 kHz with negative damping can be identified, but their damping under different h varies significantly. When h = 32, the damping of all high-frequency modes even becomes negative, yielding an incorrect stability assessment result. As a result, the selection of h imposes uncertain impacts on the algorithm performance of the conventional DMD involving both computation time and mode identification, but h can only be set manually based on experience without theoretical interpretation.

For the performance of the proposed DL-DMD as shown in the right side of Fig. 11, in addition to significantly improving the computation speed, the impact of the only tunable parameter c (truncation number) on the computation time of the DL-DMD method is regular, i.e., the computation time shortens as c decreases. As shown in the right side of Fig. 11(b), the damping and frequency of identified modes are accurate and almost identical with different c, indicating that the tuning of c also does not affect the accuracy of the mode identification results. These properties benefit from the explicit bandwidth-oriented interpretation of c as mentioned in Fig. 5. However, it is worth mentioning that decreasing c will also limit the maximum frequency f_{max} of identifiable modes as shown in Fig. 8, so reasonable truncation can be performed when there is a high requirement for computational speed and a clear upper limit of the oscillation frequency of interest. In summary, the fast computational speed and high accuracy independent of parameters make the proposed DL-DMD method more practical for oscillation detection.

To verify the noise immunity, Gaussian noise is superimposed on the measured signal to obtain test signals under different signal-to-noise ratios (SNR), as shown in Fig. 12. The corresponding mode identification results via the conventional DMD method (h = 640) and the proposed DL-DMD method (c = 80) are given in Fig. 13(a) and Fig. 13(b) respectively, showing that the damping and frequency of five dominant high-frequency oscillation modes will deviate from original values as the noise power increases (i.e. SNR decreases). Moreover, it can be found that the deviation degree of oscillation modes identified by DMD and DL-DMD are different, which also reflects noise sensitivity. To quantitatively express the noise sensitivity of different methods, the Euclidean distance between the deviated modes and the original modes in the complex plane is calculated and denoted as the deviation distance, while the average of the deviation distances of all dominant modes is defined as the metric of noise sensitivity. Fig. 13(c) shows that the noise sensitivity of DL-DMD is lower than that of DMD under different SNRs, indicating its stronger noise immunity. It is worth mentioning that, even with considerable noise power (SNR = 20 dB), the dominant oscillation modes identified by both DMD and DL-DMD can remain in the right-half plane (with negative damping), so the unstable state of the system can still be detected correctly, which benefits from the singular value decomposition step for extracting the main features.

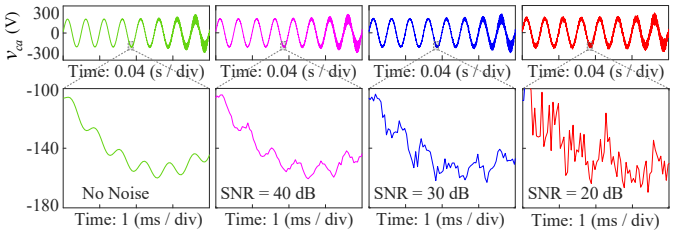

Fig. 12. Experimental signals with different signal-to-noise ratios (SNR).

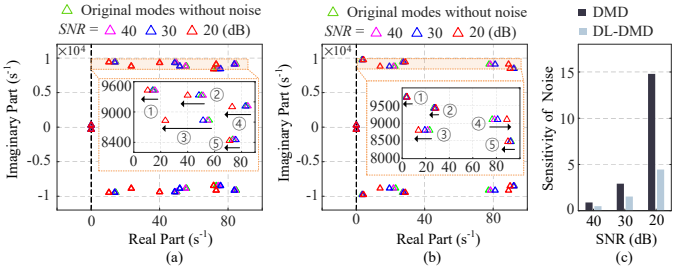

Fig. 13. Mode identification results of experimental signals under different SNR and corresponding zoom-in views when using (a) conventional DMD and (b) proposed DL-DMD, and (c) comparison of noise sensitivity — DL-DMD has lower noise sensitivity, i.e. stronger noise immunity than DMD.

Furthermore, to examine the identification performance in the case of sudden signal changes, different voltage sags are set at the 0.13 seconds of the sampling window, as shown in Fig. 14, where the degree of voltage sag (DVS) represents the percentage of the post-sag voltage amplitude to the original voltage amplitude. The corresponding mode identification results via the conventional DMD method (h = 640) and the

TABLE II
PERFORMANCE COMPARISON OF CONVENTIONAL DMD AND PROPOSED DL-DMD METHOD.

Method / Performance	Conventional DMD [13], [14], [18]–[21]	Proposed DL-DMD
Impact of Key Parameter	Stacking number h affects identification accuracy; h affects computational speed; h does not affect the maximum identifiable frequency range; h is selected manually based on experience.	Truncation number c affects computational speed; c does not affect identification accuracy; c affects the maximum identifiable frequency range; There is a bandwidth-oriented interpretation for selecting c.
Identification Speed	Slow; It becomes slower when h is too small or too large; It increases significantly with the sampling number n.	Fast; It becomes faster when c decreases; It increases slightly with the sampling number n
Identification Accuracy	High; It decreases with the h.	High; It is not affected by c.
Immunity of Noise	Moderate; Identified modes drift more as SNR increases; Noise sensitivity is higher.	Moderate; Identified modes drift more as SNR increases; Noise sensitivity is lower.
Immunity of Sudden Change	Inferior; Identified modes drift and even vanish as DVS increases; Sensitivity of sudden change is higher.	Inferior; Identified modes drift and even vanish as DVS increases; Sensitivity of sudden change is lower.

n: number of total sampled points, h: stacking number, c: truncation number, SNR: signal-to-noise ratios, DVS: degrees of voltage sags.

proposed DL-DMD method (c = 80) are given in Fig. 15(a) and Fig. 15(b) respectively, showing that the five dominant oscillation modes will deviate from original values or even disappear as the DVS decreases, but the deviation degree of oscillation modes identified by DMD and DL-DMD are different. For example, when using DMD in the worst case of voltage sags (DVS = 0%), the 3rd, 4th and 5th dominant modes disappear and the 1st and 2nd modes move to the left-half plane (presenting wrong positive damping), thus failing to correctly assess the unstable state of the system. In comparison, when using DL-DMD in this case, the 4th and 5th dominant modes disappear, the 1st and 3rd modes move to the left-half plane, but the 2nd mode just slightly deviates from its original value and remains in the right-half plane with negative damping. The sensitivity of voltage sag can be calculated in the same way as noise sensitivity as shown in Fig. 15(c), indicating that DL-DMD has stronger robustness against sudden signal changes than DMD. However, Compared to the strong noise immunity as shown in Fig. 13(c), both DMD and DL-DMD present a large identification error when there is a severe voltage sag, due to all the data is processed as a whole without the ability to deal with local temporal changes. The multi-resolution dynamic mode decomposition (MR-DMD) algorithm used in [34] can address this problem effectively, but its computational time is long due to the recursive process in the algorithm. Therefore, proposing an oscillation mode identification method with both fast computational speed and strong robustness is one of the research scopes in the future.

C. Performance Comparison

Based on the aforementioned analysis and verification, the performance of the conventional DMD and the proposed DL-DMD for oscillation mode identification are summarized and compared in Table II to demonstrate the advantages of DL-DMD clearly. In summary, compared to the conventional DMD, the proposed DL-DMD can avoid manual data stacking, provide a clear criterion for parameter setting, improve computational speed significantly, and achieve accurate oscillation mode identification unaffected by parameters, with stronger disturbance immunity and robustness.

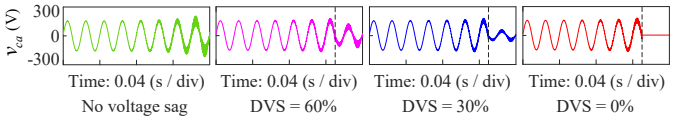

Fig. 14. Experimental signals with different degrees of voltage sags (DVS).

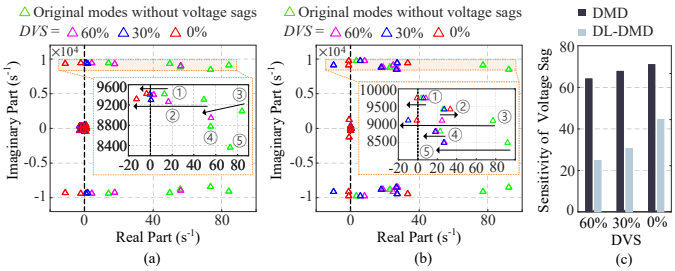

Fig. 15. Mode identification results of experimental signals under different DVS and corresponding zoom-in views when using (a) conventional DMD and (b) proposed DL-DMD — identification accuracy of both DMD and DL-DMD is significantly affected by sudden voltage sags, but DL-DMD has stronger robustness against voltage sags.

V. ONLINE VERIFICATIONS

To further test the effectiveness and advantages of the proposed DL-DMD method in the practical environment, an online test is performed as shown in Fig. 16, where the three-phase inverter with the GFM controller runs with the same setup as shown in Fig. 10. The sampled data is fed into the mode identification algorithm for computation after each sampling period T_{samp}, and then the output results will be updated after a period of computation time T_{com}. The algorithm is achieved in the Imperix B-BOX RCP controller using processing cores of ARM Cortex A9 1GHz 1GB DDR3 with a control frequency of 2 kHz, and the identification results can be monitored in real-time and saved by the Cockpit software.

The data is collected from the phase "a" of AC voltage v_{ca} with a sampling frequency of 5 kHz and a sampling period T_{samp} of 0.08 seconds, so the number of total sampled points n for each computation is 400. Further, for the DL-DMD method, the total group number q and the number of sampled

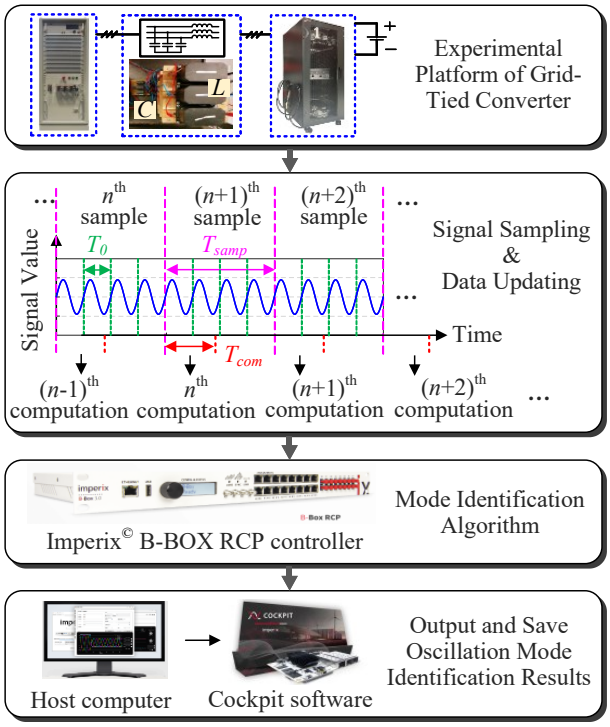

Fig. 16. Online test process of DL-DMD method for oscillation mode identification (T_{samp}: sampling period, T_{com}: computation time of the DL-DMD identification algorithm, T_0: fundamental frequency period).

points p in each data group can be calculated according to (8) as $q = 4$ and $p = 100$, while the truncation number c is set as 40. The DMD method with a stacking number $h = 80$ is also implemented as a comparison.

As shown in Fig. 17, the output identification results of DL-DMD and DMD are updated as the sampled signal varies, where stability assessment indicator and oscillation frequency of the dominant mode are used to intuitively visualize the system stability assessment results in numerical form. The stability assessment indicator will be assigned a value of 0 or 1 according to whether there are right half-plane modes with negative damping or not, which can reflect the change in system stability. The computation trigger point is used to mark the end moment of sampling and the beginning moment of the computation. Thus, the span between the computation trigger point and the updating moment of the identification results is the computation time T_{com}. As shown in Fig. 17(a), when high-frequency oscillation is provoked at 0.24 seconds, the measured voltage signal begins to present a gradual divergent waveform. After the first sampling period (from 0.24 to 0.32 seconds), DL-DMD can rapidly complete the computation within 1 millisecond to update the identification results as shown in Fig. 17(b) by the red line, indicating that the system is unstable since stability assessment indicator jumps from 0 to 1 (there are oscillation modes with negative damping), and the oscillation frequency is around 1.5 kHz. As shown in Fig. 17(b) by the blue dotted line, if the truncation number c is reduced from 40 to 25, the maximum identifiable frequency f_{max} will be decreased from 2 kHz to 1.25 kHz according to Equation (16), so the oscillation at 1.5 kHz cannot be identified, verifying the theoretical analysis about the impact of c in Section III-B. As shown in Fig. 17(c), DMD can also detect oscillation occurrence and extract oscillation frequency for stability assessment, but it requires 48 milliseconds for computation and updating results after a sampling period, which is 48 times longer than the computational time of the DL-DMD. Therefore, the online test verifies that the proposed DL-DMD has a much faster computational speed than the conventional DMD.

The shorter computation time of the proposed DL-DMD method is a significant advantage since it facilitates fast oscillation detection, and the identified modes can be promptly used for subsequent damping control to mitigate oscillations. To be specific, when the identification results show that no negative damped mode exists, the additional damping control branch can be disconnected to avoid its side effects such as adverse impacts on the dynamic characteristics. Whereas, when negative damped modes are identified, the damping control can be triggered immediately to suppress oscillations and minimize hazards. In addition, the identified damping and frequency information can be used to optimize control parameters adaptively to improve damping performance. All of the aforementioned applications require high identification speed, which demonstrates the potential usefulness of this work. Integrating mode identification into damping control is one of the scopes of future work.

VI. Conclusion

This paper proposes a novel DL-DMD method for oscillation mode identification inspired from HSS theory. Identification results based on the composite signal and experimentally measured signal show that the computational speed of the proposed method is improved significantly with high identification accuracy and noise immunity, compared to the conventional DMD method. In addition, the empirical parameter setting with uncertain impacts is avoided, while bandwidth-oriented interpretation for parameter selection is provided. By further online tests, the effectiveness and advantages of the proposed DL-DMD method are verified, which is practical for rapid oscillation detection in grid-tied converter systems. To extend the scope in the future, the identified modes will be exploited for further control measures to mitigate instabilities.

References

[1] Y. Cheng, L. Fan, J. Rose, S.-H. Huang, J. Schmall, X. Wang, X. Xie, J. Shair, J. R. Ramamurthy, N. Modi, C. Li, C. Wang, S. Shah, B. Pal, Z. Miao, A. Isaacs, J. Mahseredjian, and J. Zhou, "Real-world subsynchronous oscillation events in power grids with high penetrations of inverter-based resources," *IEEE Trans. Power Syst.*, vol. 38, no. 1, pp. 316–330, 2023.

[2] L. Kong, Y. Xue, L. Qiao, and F. Wang, "Review of small-signal converter-driven stability issues in power systems," *IEEE Open Access J. Power Energy.*, vol. 9, pp. 29–41, 2022.

[3] Y. Gu and T. C. Green, "Power system stability with a high penetration of inverter-based resources," *Proc. IEEE*, vol. 111, no. 7, pp. 832–853, July 2023.

[4] X. Wang and F. Blaabjerg, "Harmonic stability in power electronic-based power systems: Concept, modeling, and analysis," *IEEE Trans. Smart Grid.*, vol. 10, no. 3, pp. 2858–2870, 2019.

[5] M. Zhao, H. Yin, Y. Xue, X. Zhang, and Y. Lan, "Coordinated damping control design for power system with multiple virtual synchronous generators based on Prony method," *IEEE Open Access J. Power Energy.*, vol. 8, pp. 316–328, 2021.

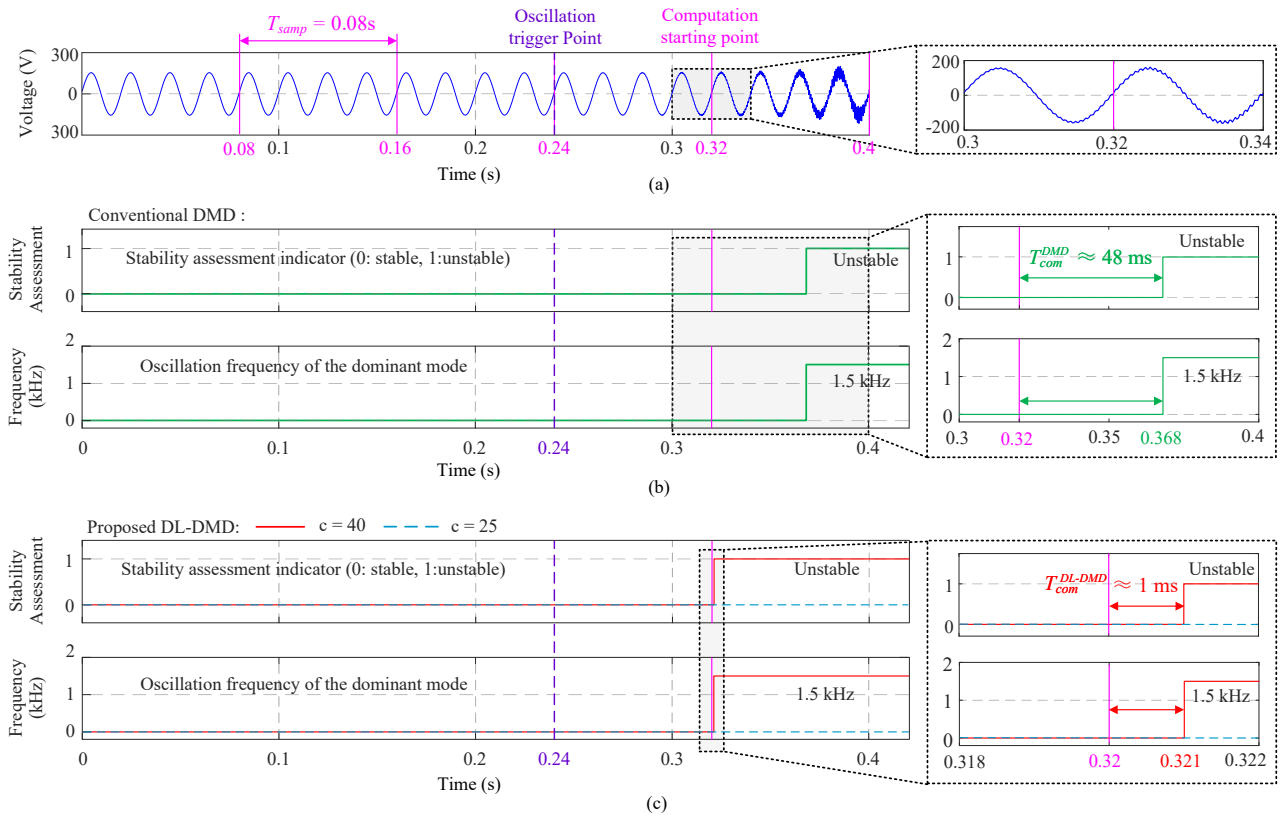

Fig. 17. Online experimental results of conventional DMD and proposed DL-DMD method for stability assessment — DL-DMD can identify oscillation within 1 ms, which is significantly faster than DMD, and the identifiable frequency range of DL-DMD is determined by the truncation number c.

[6] Q. Peng, G. Buticchi, N. M. L. Tan, S. Guenter, J. Yang, and P. Wheeler, "Modeling techniques and stability analysis tools for grid-connected converters," *IEEE Open J. Power Electron.*, vol. 3, pp. 450–467, 2022.

[7] H. Zhang, L. Harnefors, X. Wang, H. Gong, and J.-P. Hasler, "Stability analysis of grid-connected voltage-source converters using SISO modeling," *IEEE Trans. Power Electron.*, vol. 34, no. 8, pp. 8104–8117, 2019.

[8] X. Gao, D. Zhou, A. Anvari-Moghaddam, and F. Blaabjerg, "Stability analysis of grid-following and grid-forming converters based on state-space modelling," *IEEE Trans. Ind Appl.*, vol. 60, no. 3, pp. 4910–4920, 2024.

[9] J. Mace, A. Cervone, and D. Dujic, "Self-synchronized grid impedance estimation unit using interpolated DFT technique," *IEEE Trans. Power Electron.*, vol. 39, no. 4, pp. 4624–4635, 2024.

[10] H. Gong, X. Wang, and D. Yang, "DQ-frame impedance measurement of three-phase converters using time-domain mimo parametric identification," *IEEE Trans. Power Electron.*, vol. 36, no. 2, pp. 2131–2142, 2021.

[11] E. O. Brigham and R. E. Morrow, "The fast Fourier transform," *IEEE Spectrum*, vol. 4, no. 12, pp. 63–70, 1967.

[12] J. Yi, Y. Gao, M. Wang, J. Zhu, J. Ma, W. Shi, and H. Wang, "Research on APF based on adaptive analysis instantaneous reactive power harmonic detection method," vol. 6, 2023, pp. 578–582.

[13] P. J. Schmid, "Dynamic mode decomposition of numerical and experimental data," *J. Comput. Dyn.*, vol. 656, pp. 5–28, 2010.

[14] P. J. Schmid, "Dynamic mode decomposition and its variants," *Ann. Rev. Fluid Mech.*, vol. 54, pp. 225 – 254, January 2022.

[15] R. Tapia-Olvera, D. Guillen, F. Beltran-Carbajal, and L. M. Castro, "An adaptive scheme to improve Prony's method performance to estimate signal parameters of power system oscillations," *IEEE Trans. Instrum Meas.*, vol. 71, pp. 1–12, 2022.

[16] G. E. Mejia-Ruiz, R. Cárdenas-Javier, M. R. Arrieta Paternina, J. R. Rodríguez-Rodríguez, J. M. Ramirez, and A. Zamora-Mendez, "Coordinated optimal volt/var control for distribution networks via D-PMUs and EV chargers by exploiting the eigensystem realization," *IEEE Trans. Smart Grid.*, vol. 12, no. 3, pp. 2425–2438, 2021.

[17] H. Ye, Y. Song, Z. Zhang, and C. Wen, "Global dynamic event-triggered control for nonlinear systems with sensor and actuator faults: A matrix pencil based approach," *IEEE Trans. Automat Contr.*, vol. 69, no. 3, pp. 2007–2014, 2024.

[18] A. Alassaf and L. Fan, "Randomized dynamic mode decomposition for oscillation modal analysis," *IEEE Trans. Power Syst.*, vol. 36, no. 2, pp. 1399–1408, March 2021.

[19] E. Barocio, B. C. Pal, N. F. Thornhill, and A. R. Messina, "A dynamic mode decomposition framework for global power system oscillation analysis," *IEEE Trans. Power Syst.*, vol. 30, no. 6, pp. 2902–2912, 2015.

[20] B. N. Kumar, S. B. Karanki, and M. S. Manikandan, "Dynamic mode decomposition based approach for accurate measurement of voltage flicker components," *IEEE Trans. Instrum Meas.*, vol. 72, pp. 1–10, February 2023.

[21] D. Yang, B. Wang, G. Cai, Z. Chen, J. Ma, Z. Sun, and L. Wang, "Data-driven estimation of inertia for multiarea interconnected power systems using dynamic mode decomposition," *IEEE Trans. Ind. Inf.*, vol. 17, no. 4, pp. 2686–2695, 2021.

[22] J. H. Tu, C. W. Rowley, D. M. Luchtenburg, S. L. Brunton, and J. N. Kutz, "On dynamic mode decomposition: Theory and applications," *J.Comput. Dyn.*, vol. 1, no. 2, pp. 391–421, 2014.

[23] F. Andreuzzi, N. Demo, and G. Rozza, "A dynamic mode decomposition extension for the forecasting of parametric dynamical systems," *SIAM J. Appl. Dyn. Syst.*, vol. 22, no. 3, pp. 2432–2458, 2023.

[24] A. Alassaf and L. Fan, "Dynamic mode decomposition in various power system applications," in *North Am. Power Symp.*, 2019, pp. 1–6.

[25] E. V. Filho and P. Lopes dos Santos, "A dynamic mode decomposition approach with hankel blocks to forecast multi-channel temporal series," *IEEE Control Syst Lett.*, vol. 3, no. 3, pp. 739–744, 2019.

[26] N. M. Wereley, "Analysis and control of linear periodically time varying systems," Ph.D. dissertation, Dept. Aeronaut. Astronaut., MIT, Cambridge, MA, USA, 1991.

[27] V. Salis, A. Costabeber, S. M. Cox, P. Zanchetta, and A. Formentini, "Stability boundary analysis in single-phase grid-connected inverters with PLL by LTP theory," *IEEE Trans. Power Electron.*, vol. 33, no. 5, pp. 4023–4036, 2018.

[28] J. Lyu, X. Zhang, X. Cai, and M. Molinas, "Harmonic state-space based small-signal impedance modeling of a modular multilevel converter with consideration of internal harmonic dynamics," *IEEE Trans. Power Electron.*, vol. 34, no. 3, pp. 2134–2148, 2019.

[29] J. Zhang, X. Yang, W. Chen, H. Zhou, and J. Luo, "A multifrequency small-signal model for the MLCL-filtered grid-connected inverter considering the fce of nonlinear inductors," *IEEE Trans. Ind Electron.*, vol. 70, no. 5, pp. 4901–4911, 2023.
[30] Y. Cai, Y. He, H. Zhang, H. Zhou, and J. Liu, "Research on harmonic state-space modeling and calculation analysis of low-switching-frequency grid-connected inverter considering the impact of digitization," *IEEE Trans. Power Electron.*, vol. 38, no. 1, pp. 1003–1021, January 2023.
[31] Y. Liao, H. Sandberg, and X. Wang, "Vector-norm based truncation of harmonic transfer functions in black-box electronic power systems," *IEEE Open J. Ind. Electron. Soc.*, vol. 3, pp. 163–173, 2022.
[32] L. Harnefors, R. Finger, X. Wang, H. Bai, and F. Blaabjerg, "Vsc input-admittance modeling and analysis above the Nyquist frequency for passivity-based stability assessment," *IEEE Trans. Ind Electron.*, vol. 64, no. 8, pp. 6362–6370, 2017.
[33] Y. Liao, X. Wang, and F. Blaabjerg, "Passivity-based analysis and design of linear voltage controllers for voltage-source converters," *IEEE Open J. Ind. Electron. Soc.*, vol. 1, pp. 114–126, 2020.
[34] R. Kong, S. Sahoo, Y. Song, Y. Xiao, C. Gao, and F. Blaabjerg, "Multi-resolution dynamic mode decomposition for wideband harmonic instability identification," *IEEE Trans. Power Electron.*, pp. 1–15, 2024.

Rui Kong (S'23) received the B.Sc. and M.Eng. degrees in Electrical Engineering from Southwest Jiaotong University, Chengdu, China, in 2019 and 2022, respectively. He is currently working toward a Ph.D. degree in the Department of Energy, Aalborg University (AAU Energy), Aalborg, Denmark.

His research interests include the data-driven identification and control, modeling, and stability analysis of power electronic converter-based systems.

Subham Sahoo (S'16–M'18–SM'23) received the B.Tech. & Ph.D. degree in Electrical and Electronics Engineering from VSSUT, Burla, India and Electrical Engineering at Indian Institute of Technology, Delhi, New Delhi, India in 2014 & 2018, respectively. He is currently an Assistant Professor in the Department of Energy, Aalborg University (AAU), Denmark, where he is also the vice-leader of the research group on Reliability of Power Electronic Converters (ReliaPEC) in AAU Energy.

He is a recipient of the Indian National Academy of Engineering (INAE) Innovative Students Project Award for the best PhD thesis in 2019. He is also selected into EU-US National Academy of Engineering (NAE) Frontier of Engineering (FOE) Class of 2021. He is an affiliate of the Danish Data Science Academy (DDSA), European Lab for Learning & Intelligent Systems (ELLIS) and Lundbeck Foundation Investigator Network. He was also a distinguished reviewer for IEEE Transactions on Smart Grid in 2020. He is currently the vice-chair of IEEE PELS Technical Committee (TC) 10 on Design Methodologies. He is an Associate Editor on IEEE Transactions on Transportation Electrification.

His research interests are control, optimization, cybersecurity and stability of power electronic dominated grids, application of artificial intelligence and machine learning in power electronic systems.

Shuyu Ou (S'22) received the B.Sc. and M.Sc. degrees in electrical engineering from South China University of Technology, Guangzhou, China, in 2017, and Royal Institute of Technology, Stockholm, Sweden, in 2019, respectively. He is currently working toward the Ph.D. degree in Electrical Engineering with Aalborg University, Aalborg, Denmark, funded by European Union's Horizon 2020 research and innovation program. From 2019 to 2022, he was with Huawei Sweden Research Center, Sweden. His research interests include reliability and data-driven condition monitoring of power electronic converters.

Xiangyu Meng (S'20) received the B.S. degree in electrical engineering and automation from Lanzhou Jiaotong University, Lanzhou, China, in 2019. He is currently working toward the Ph.D. degree in electrical engineering with the School of Electrical Engineering, Southwest Jiaotong University, Chengdu, China. From 2024, he is a joint-cultivated Ph.D. with the Department of Electrical and Electronic Engineering, University of Manchester,Manchester, U.K. His current research focuses on stability analysis in single-phase vehicle-grid systems.

Guoqing Gao (S'19) received the B.S. degree from Xidian University, Xi'an, China, in 2017, the M.S. degree from Xi'an Jiaotong University, Xi'an, China, in 2020, and the Ph.D. degree from Aalborg University, Aalborg, Denmark in 2024, all in electrical engineering. His research interests include control, protection, and stability analysis of power electronic converter interfaced grids; modeling, control, and stability analysis of power electronic converters.

Frede Blaabjerg (S'86–M'88–SM'97–F'03) received the Ph.D. degree in electrical engineering from Aalborg University, Aalborg, Denmark, in 1995. He was with ABB-Scandia, Randers, Denmark, from 1987 to 1988. He became an Assistant Professor in 1992, an Associate Professor in 1996, and a Full Professor of power electronics and drives in 1998. From 2017 he became a Villum Investigator. He is honoris causa at University Politehnica Timisoara (UPT), Romania, and Tallinn Technical University (TTU) in Estonia. His current research interests include power electronics and its applications, such as in wind turbines, PV systems, reliability, harmonics, and adjustable speed drives. He has published more than 600 journal papers in the fields of power electronics and its applications. He is the co-author of four monographs and editor of ten books in power electronics and its applications.

He has received 32 IEEE Prize Paper Awards, the IEEE PELS Distinguished Service Award in 2009, the EPE-PEMC Council Award in 2010, the IEEE William E. Newell Power Electronics Award 2014, the Villum Kann Rasmussen Research Award 2014, the Global Energy uPrize in 2019 and the 2020 IEEE Edison Medal. He was the Editor-in-Chief of the IEEE TRANSACTIONS ON POWER ELECTRONICS from 2006 to 2012. He has been a Distinguished Lecturer for the IEEE Power Electronics Society from 2005 to 2007 and for the IEEE Industry Applications Society from 2010 to 2011 as well as 2017 to 2018. In 2019-2020 he served as President of the IEEE Power Electronics Society. He is Vice-President of the Danish Academy of Technical Sciences too. He is nominated in 2014-2019 by Thomson Reuters to be between the most 250 cited researchers in Engineering in the world.